npj | climate and atmospheric science

Article

Published in partnership with CECCR at King Abdulaziz University

https://doi.org/10.1038/s41612-024-00628-y

Synergistic effect of boreal autumn SST over the tropical and South Pacific and winter NAO on winter precipitation in the southern Europe

Xinxin Tang[1] & Jianping Li[1,2]

We find a positive phase of meridional tripole pattern of boreal autumn sea surface temperature anomalies over the tropical and South Pacific (TSPT+) has a synergistic effect with winter negative NAO (NAO−) on the amplitude and occurrence of winter precipitation in southern Europe (SEWP). This synergistic effect is attributed to the linear superposition and nonlinear effect of winter NAO− and preceding autumn TSPT+. The autumn TSPT+ can persist into winter, and the winter TSPT+ with NAO− can stimulate a greater amount of Rossby wave energy propagating to the North Atlantic-Europe (NAE) region than without NAO−, and thereby synergistically regulating circulation with winter NAO−. Thus, winter NAO− and autumn TSPT+ have a synergistic effect on the northwest-southeast trending positive-negative-positive winter circulation over the NAE region. Driven by the intensified mean circulation, water vapor transports and storm activity over southern Europe are evidently strong, which is in favor of SEWP formation.

As the main aspect of the influence on the European climate is the North Atlantic Oscillation (NAO) variability. The NAO is a seesaw in pressure between the subpolar Icelandic low and the subtropical Azores high regions of the North Atlantic Ocean. It is now known to fundamentally arise from the internal atmospheric dynamics of wave–wave and/or wave–mean flow interaction[1,2], and NAO is associated with the North Atlantic storm track[3]. During positive phase of NAO, the storm track strengthened over Scandinavia, weakened over southern Europe, and vice versa. Also, it is clear that NAO has variability on weather and seasonal time scales, which is strongly influenced by anomalies of the stratospheric polar vortex on a week time scale[4]. Further, it has been shown that interannual variability of the NAO arises primarily from climate "noise" and does not require forcing external to the atmosphere[1]. The variability of NAO is also influenced by the tropical Atlantic[5–7] and tropical Pacific Sea surface temperature anomalies (SSTA)[8,9] through the atmospheric bridge of Rossby waves.

The impact of NAO on Europe is known that positive NAO phases are characterized by lower-than-average precipitation over large areas of southern Europe and the Mediterranean, whereas negative phases of NAO are associated with wetter conditions, which is related to the heat and moisture transport and furthermore, the changes of the Atlantic storm tracks[10–14]. The greatest influence of NAO on precipitation is in Western Europe, enhancing precipitation from France across the British Isles to Scandinavia and is a reason for low totals in Spain[15]. The notable influence of NAO on European precipitation is expected mainly during the winter months[16,17].

Although NAO is of prime importance in order to understand the precipitation variability in the South Europe, it is not the only mode of variability with significant effects[18–20]. The tropical North Atlantic SST is related to the winter precipitation of south-eastern Europe through the atmospheric circulation processes[21]. Also, many studies have investigated the influence of Pacific Ocean on South Europe and Mediterranean region. ENSO is an important interannual climate variability influencing precipitation over North Atlantic-Europe (NAE) region[22–24]. Previous studies have found increased wintertime precipitation over Britain, France, and Germany during an El Niño, but decreased precipitation over Scandinavia[25]. However, some analyses during boreal winter reveal little effect of coincident ENSO conditions on either European precipitation or upper tropospheric conditions over Europe[26–29]. These seemingly contradictory

[1]Frontiers Science Center for Deep Ocean Multi-spheres and Earth System (DOMES)/Key Laboratory of Physical Oceanography/Academy of Future Ocean/College of Oceanic and Atmospheric Sciences/Center for Ocean Carbon Neutrality, Ocean University of China, Qingdao 266100, China. [2]Laoshan Laboratory, Qingdao 266237, China. e-mail: ljp@ouc.edu.cn

conclusions result from the fact that the ENSO impacts over the NAE region are associated with highly nonlinear dynamics[30,31] and the signal-to-noise ratio in the early-winter response to El Niño[32]. Therefore, considering the isolated ENSO signal is not comprehensive to understand the variability of European winter precipitation. Also, studies found that the influence of ENSO on winter Europe is modulated by North Pacific Climate[19,33]. Although studies have revealed the influence of tropical and North Pacific Ocean on Europe, the analysis of South Pacific Ocean on winter Europe is not evaluated. Studies have found that preceding boreal autumn SSTA in South Pacific Ocean have significant influence on boreal winter precipitation in the North America region[34] and East Asia[35] through interhemispheric Rossby wave train simulated by SSTA over South Pacific Ocean. The result motivates us to ask whether tropical and south Pacific SSTA in the preceding season, influences South European winter precipitation (SEWP). Considering that winter NAO is a major factor influencing SEWP, it is of interest to investigate whether preceding SSTA pattern and winter NAO have a synergistic effect on the SEWP.

The concept of synergistic effect is adopted form Li et al.[36] that a joint effect of two factors is significantly stronger than the maximum of isolated effects. Particularly, this concept of synergistic effect has been widely used to understand the variability of climate[37,38] and extreme climate[39–41]. Therefore, we adopt the concept of synergistic effect in Li et al.[36] to investigate whether the joint events of winter negative NAO and preceding season SSTA produces significantly stronger and more frequent occurrence of winter precipitation than they occur in isolation to better understand the influencing mechanism of SEWP variability. However, the mechanism of synergistic effect interpreted by former studies have not involved the contribution of linear and nonlinear effects. If two factors are independent, we assume that response of combined events is the linear superposition of their isolated effects. The climate, being a nonlinear system, prompts us to investigate whether the combined events contribute more significantly than the superposition of their isolated events. If this is the case, there may be an unexpected amplification due to non-linearity, which we define as a nonlinear effect in this study.

Therefore, this study evaluates the synergistic effect of boreal winter negative NAO and preceding autumn SSTA on SEWP, and describe the underlying dynamical mechanisms in terms of contribution of linear superposition effect and nonlinear effect. We will access large-scale circulation and dynamics, including pathways of Rossby wave energy and numerical experiment. Further, mechanisms of the synergistic effect of autumn SSTA and winter NAO on SEWP formation in terms of moisture transport and transient eddies will be evaluated. Collectively, this will provide a more complete understanding of SEWP variability.

Results

Relationship of winter (DJF) SEWP with NAO and SSTA

The relationship between the winter NAO and winter precipitation over Europe has long been known, as displayed in Fig. 1. For simplicity, hereafter the NAO refers to winter NAO unless specified otherwise, and X + (−) denotes the positive (negative) phase of the event X. It can be seen from Fig. 1 that a dipole mode of precipitation anomaly with positive (negative) anomalies in the northern (southern) Europe is associated with the positive phase of NAO[12,42]. Thus, the NAO has a strong relationship with southern Europe winter precipitation (SEWP; the black box in Fig. 1a; 36°–52°N, 10°W–45°E), with a correlation of −0.71. However, not all negative NAO (NAO−) events correspond to anomalous wet SEWP, and SEWP is also influenced by other factors, such as preceding SSTA[43]. To explore the preceding SSTA that have synergistic effect with NAO− on the occurrence of SEWP, SEWP anomalies during the joint events of NAO− and SON (DJF) SSTA+ and those of NAO− and SON (DJF) SSTA− are compared (Fig. 1b, c). We find a NAO− with a positive phase of meridional tripole pattern of SON SSTA over the tropical and South Pacific (TSPT +) that has cold SSTA in the subtropical southwest Pacific and warm SSTA in the tropical Pacific and mid-latitude South Pacific will produce stronger SEWP anomalies than that with the SON TSPT− that has warm SSTA in the subtropical southwest Pacific and cold SSTA in the tropical Pacific and mid-latitude South Pacific. For the sake of simplicity, hereafter the TSPT refers to boreal autumn TSPT unless otherwise stated. The SEWP during the joint events of NAO− and TSPT+ (NAO−⊕TSPT+) is stronger than those during the isolated events of NAO− (NAO−\TSPT+) and TSPT+ (TSPT+ \NAO−). To further evaluate relationship between the TSPT, NAO and SEWP, an TSPT index is defined as the difference between the standardized averaged SON SSTA over the positive SSTA regions (the black solid rectangle A {5°S-5°N, 185°E-245°E} and C {40°S-57°S, 190°E-220°E} in Fig. 1b) and the negative SSTA region (the black dashed rectangle B {18°S-35°S, 160°E-200°E} in Fig. 1b), based on the formula: TSPT index = (1/4{A} + 1/4{C})−1/2{B}, where {A}, {B} and {C} denote areal averaged SSTA in the boxes A, B and C, respectively. Figure 1e shows that the TSPT-like SSTA in winter is closely related to autumn TSPT, indicating that TSPT in boreal autumn can persist into winter and in turn influence SEWP through the combination with NAO−.

Figure 2 shows the time series of the NAO, TSPT and SEWP indices, and scatter plot of SEWP for NAO and TSPT. Classification of years for isolated and joint events of NAO− and TSPT+ is shown in Supplementary table 1, in which winter years are defined based on the year of December. As shown in Fig. 2b, TSPT+ and NAO− are conductive to abnormally stronger SEWP, and NAO have stronger relationship with SEWP than TSPT. SEWP anomalies during NAO−⊕TSPT + is 16.18 mm, which is much stronger than those during NAO−\TSPT + (7.39 mm), and TSPT + \NAO− (−0.59 mm). Thus, there might be an implicit synergistic effect[36] between NAO− and TSPT+ on SEWP. Furthermore, the proportion of years with positive SEWP anomalies to total years for NAO−\TSPT + and TSPT + \NAO− are 80% and 35.7%, respectively. However, a 100% proportion of increased SEWP is observed during NAO−⊕TSPT + (Fig. 2b). Thus, NAO− with TSPT+ is more accurately indicative of SEWP increase than without TSPT + . In addition, both NAO and TSPT show interannual variation with a correlation coefficient of −0.23 (Fig. 2a), and the linear relationship between SEWP and TSPT is relatively weak, with a correlation coefficient of 0.26. Therefore, it is difficult to discover the potential relationship between TSPT and NAO with SEWP using only linear correlation, since nonlinear effects cannot be taken into account. Instead, it is pertinent to explore the synergistic effects of TSPT+ and NAO− on SEWP through composite analysis (Fig. 1b, c).

Figure 3 shows spatial distribution of DJF precipitation during isolated and joint events of NAO− and TSPT + . Regionally, significant positive land DJF precipitation anomalies around the Mediterranean and particularly in the Iberian Peninsula and Mountains east of the Adriatic Sea is related to NAO− (Fig. 3a), which is consistent with the result in Fig. 1a. Weak wet anomaly in British Isled, Germany, and France and abnormally weak dry around Mediterranean region is associated with TSPT+ (Fig. 3b). In comparison, the influence of NAO− on SEWP is greater than that of TSPT + , and the influence of TSPT+ on SEWP is not significant. However, during the joint events, above-normal DJF precipitation throughout the study area is significantly stronger than those in the isolated events (Fig. 3c). Moreover, the strength of SEWP anomalies during NAO−⊕TSPT + are about two times that of NAO−\TSPT + events, reinforcing that NAO− and TSPT+ may have significant synergistic effects on SEWP (Fig. 3f). The sum of the responses to isolated events appears as a precipitation anomaly similar to that of NAO−\TSPT + (Fig. 3d), implying that the synergistic effect of NAO− and TSPT+ on SEWP is not only caused by their linear superposition, but also by a nonlinear effect. Figure 3e shows the evident DJF precipitation increase over the Iberian Peninsula, the Alps, northeast coast of the Mediterranean and north of the black sea which may be related to nonlinear effect of NAO− and TSPT + .

Similar results are found from the local covariance between NAO, TSPT and SEWP, that NAO− is related to SEWP increase over the Mediterranean (Fig. 4a) during NAO−\TSPT + , and TSPT+ is associated with SEWP increase over British Isled, Germany and France during TSPT + \NAO− (Fig. 4b), which is similar with that in Fig. 3. Evidently, during NAO

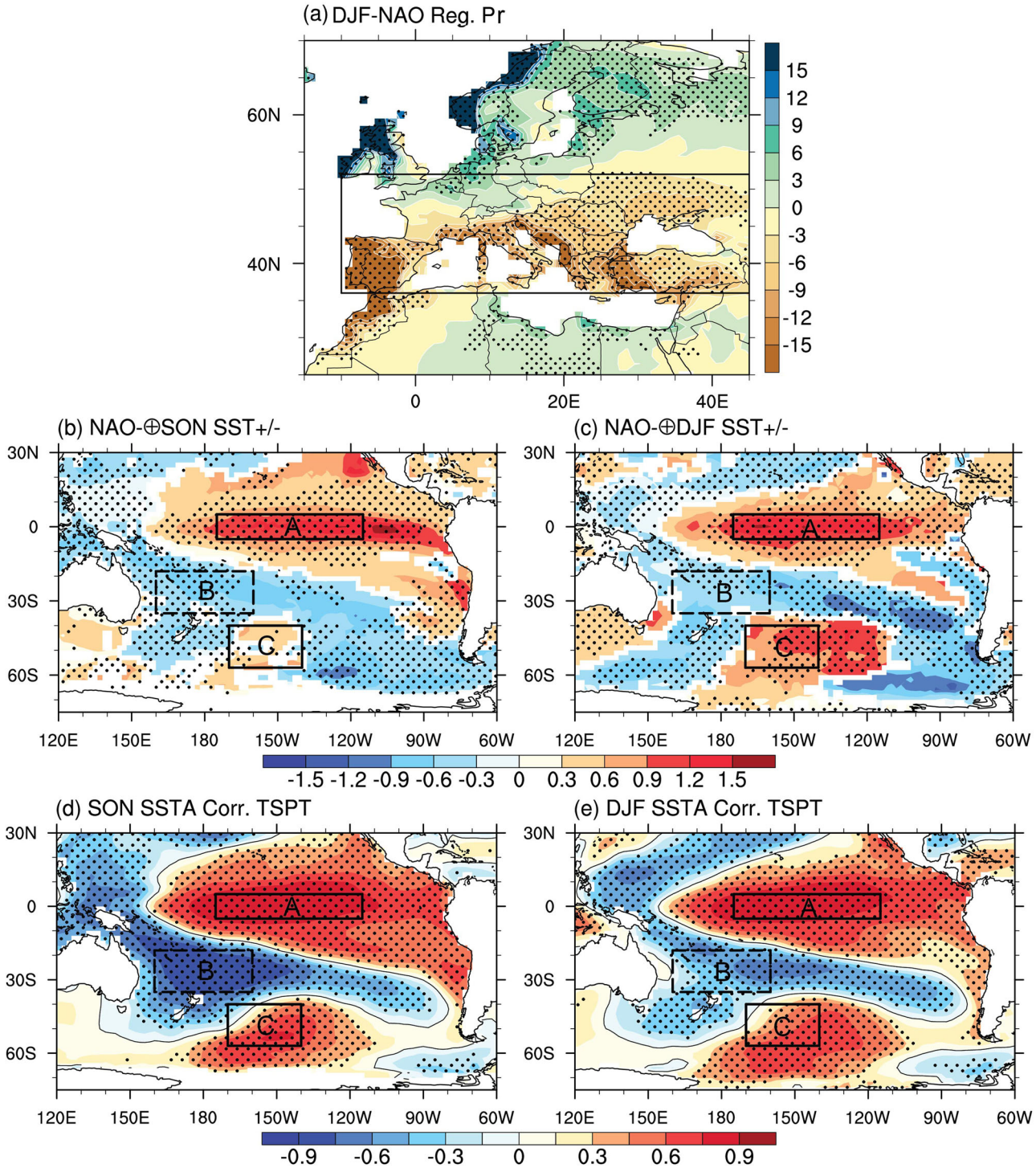

Fig. 1 | Relationship of SEWP with NAO and SSTA. a Regression map of winter (DJF) precipitation anomalies (mm) on the DJF NAO index, and composites of SSTA during the co-occurrence of NAO− and boreal autumn (SON) (**b**), DJF (**c**) warm (red shading) and clod (blue shading) Pacific SSTA events, and correlation coefficients between SON (**d**), DJF (**e**) SSTA and SON TSPT index defined by SSTA in the black boxes (see the text). The red (blue) shading in (**b**, **c**) indicates SEWP during warm (cold) SSTA and DJF NAO− events is stronger than that of cold (warm) SSTA and NAO− events. Black dotted areas in (**b**, **c**) indicate amplitudes of SEWP during joint events of NAO− and SSTA + /− are stronger than those in the isolated events of NAO− and SSTA + /−. ⊕ means joint event. Dotted areas in (**a**, **d**, **e**) are significant at or above the 95% confidence level (two-tailed Student's *t* test). A (black solid rectangle), B (black dashed rectangle) and C (black solid rectangle) in (**b**, **c**, **d**, **e**) denote the three regions in the tropical and south Pacific.

−⊕TSPT +, covariates of NAO−, TSPT + and SEWP anomalies over southern Europe exhibit significant enhancement, which is associated with that SEWP during joint events contains nonlinear effect of NAO− and TSPT+ that goes beyond their linear superposition, reinforcing that NAO− and TSPT+ have a synergistic effect on SEWP.

Synergistic effect of NAO− and TSPT+ on DJF circulation

Figure 5 shows the composite anomalies of DJF geopotential height at 500 hPa during NAO−\TSPT +, TSPT + \NAO−, NAO−⊕TSPT + events, and the linear superposition and nonlinear effect of NAO− and TSPT +, respectively. A feature of NAO− with anomalous

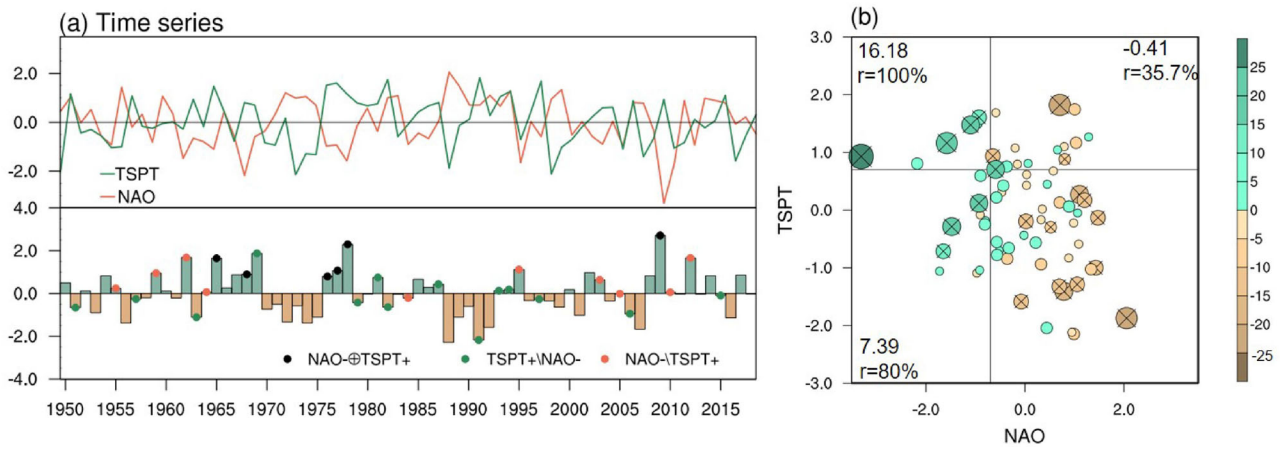

Fig. 2 | The time series of the NAO, TSPT and SEWP indices, and scatter plot of SEWP for NAO and TSPT. a The standardized seasonal mean indices of SON TSPT (green solid line), DJF NAO (orange solid line), and SEWP (shaded bars). **b** Scatter plot of SEWP for the DJF NAO [x axis in (**b**)] and SON TSPT [y axis in (**b**)]. Stronger precipitation anomalies are highlighted by larger dots in (**b**). Cross-hatched dots in (**b**) are significant at the 90% confidence level (two-tailed Student's *t* test). The three numbers in (**b**) denote SEWP averages for the isolated events of NAO−\TSPT + and TSPT + \NAO− and the joint events of NAO−⊕TSPT +, respectively. "r" in (**b**) indicates the proportion (%) of years with positive SEWP anomalies to total years for the events of NAO−\TSPT + (left bottom), TSPT + \NAO− (right top), and NAO −⊕TSPT + (left top), respectively.

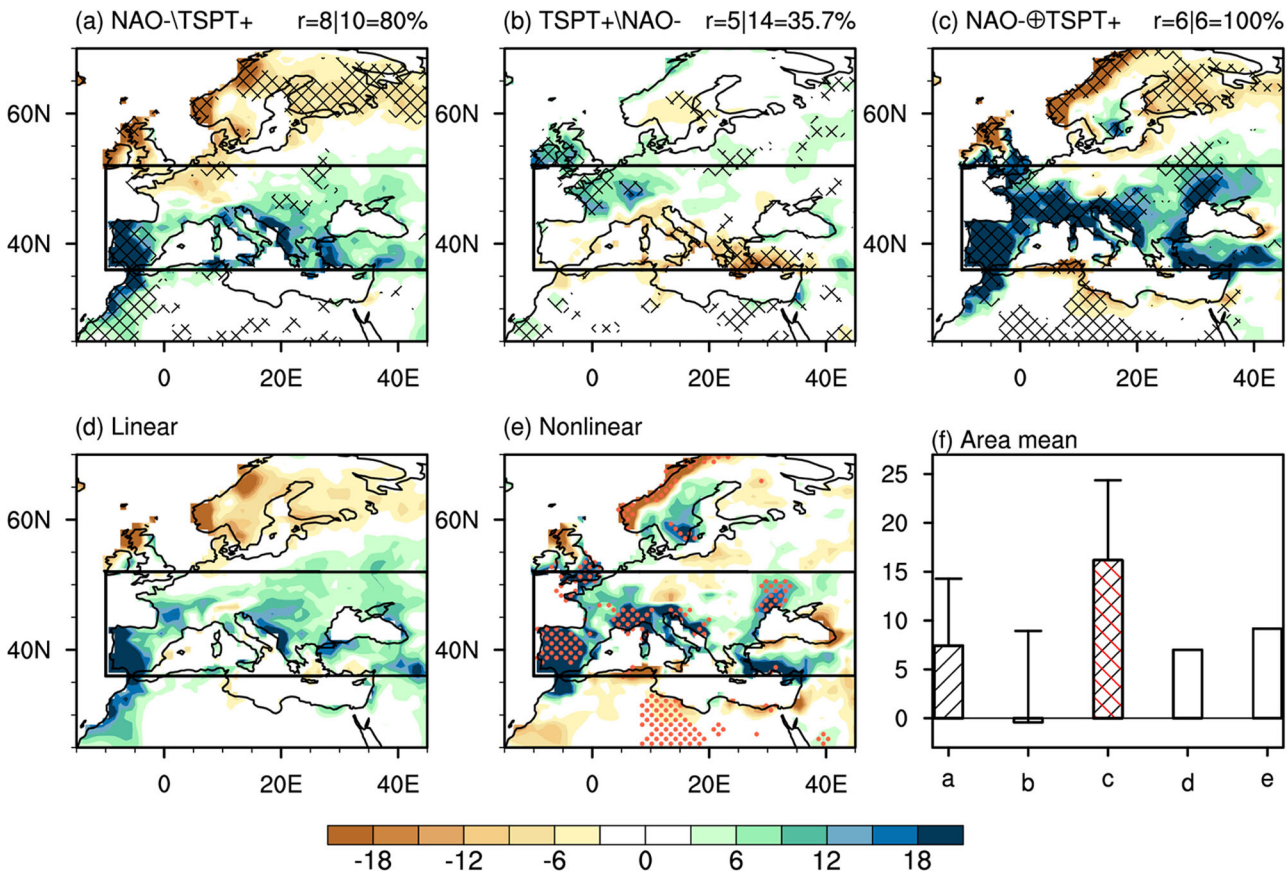

Fig. 3 | Composite anomalies of DJF precipitation. Composite mean anomalies of DJF precipitation: (**a**) NAO−\TSPT +, (**b**) TSPT + \NAO−, (**c**) NAO−⊕TSPT +, (**d**) linear superposition of (**a**) and (**b**), (**e**) difference between (**c**) and (**d**). Bars in (**f**) indicate SEWP in (**a**–**e**). Crossed areas are significant at the 90% confidence level. Red dotted areas in (**e**) indicate precipitation in (**c**) are significantly stronger than those in (**a**) and (**b**). Black slash bars in (**f**) indicate composites to climatology are significant at the 90% confidence level, and red slash bar in (**f**) indicates SEWP in (**c**) is significantly stronger than that in (**a**). The line variation over the bar indicates standard deviation.

positive–negative geopotential height over the middle and high latitudes of the North Atlantic is observed (Fig. 5a) during NAO−\TSPT + [44–46]. During TSPT + \NAO−, an anomalous low appears in north Europe and anomalously weak high pressure occurs in North Africa and mid latitude Central Asia (Fig. 5b). In addition, A Pacific-North American-like wave train is observed, with an abnormally low occurring over southeastern North America and Bermuda, and extends northeastward connecting with the low across southern Europe (Fig. 5b). The sum of

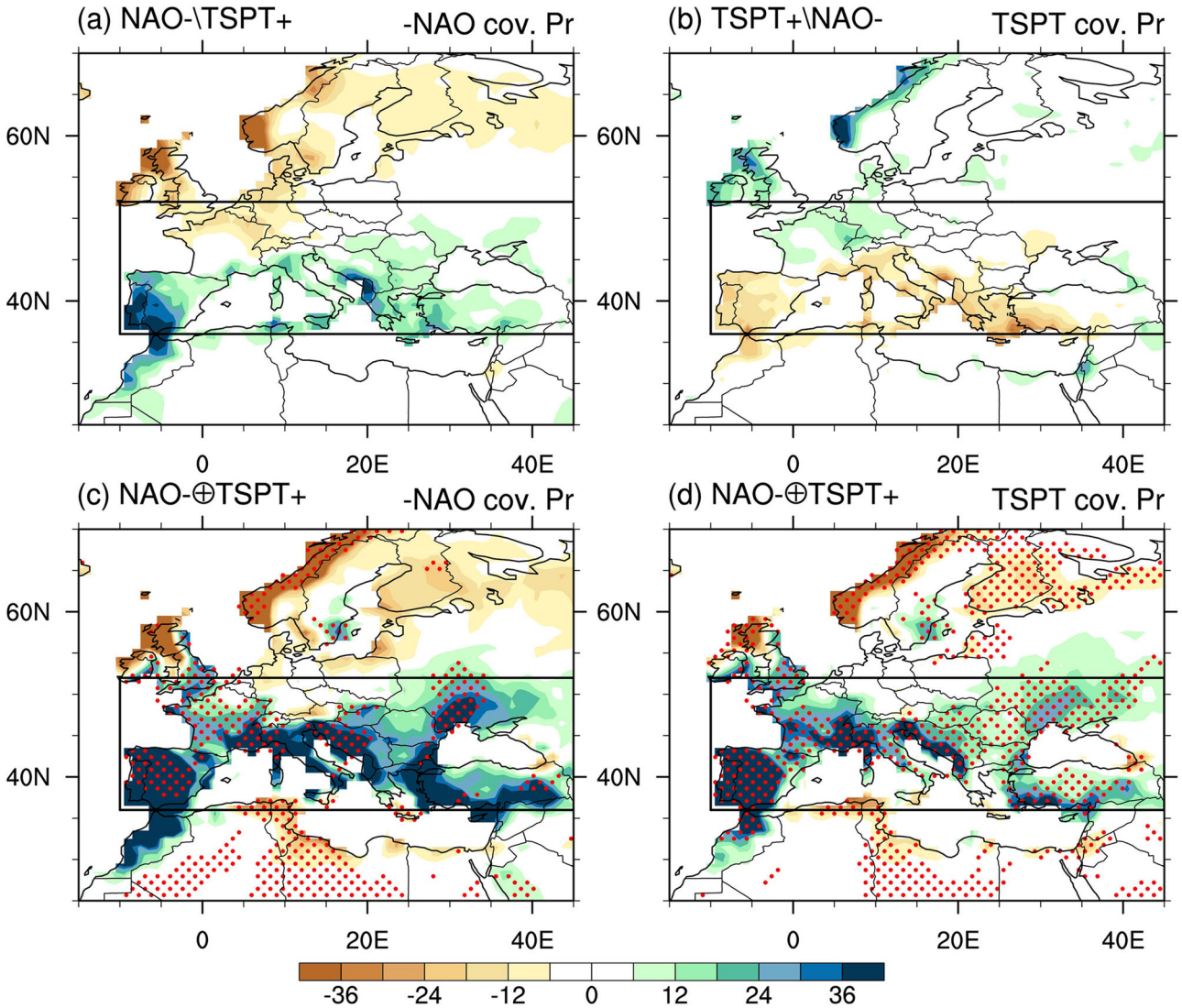

Fig. 4 | Local covariance between DJF precipitation and NAO, TSPT. Local covariance between DJF precipitation anomalies and indices of DJF NAO (*−1; left panels) and SON TSPT (right panels) under NAO−\TSPT + (**a**), TSPT + \NAO− (**b**), and NAO−⊕TSPT + (**c**, **d**). The red dotted areas in (**c**) and (**d**) are significantly different from that in (**a**) and (**b**) at the 90% confidence level determined by bootstrap method, respectively.

isolated responses to NAO− and TSPT+ over the NAE region is similarly with that of NAO−\TSPT +, which is corresponded to the linear superposition effect on SEWP (Fig. 4d). Significantly, a strengthened tripole circulation anomaly exhibiting northwest-southeast trend, with a low in midlatitude North Atlantic, and anomalously high over Greenland and Baffin Island, and North Africa and the Caspian Sea is observed during NAO−⊕TSPT + (Fig. 5c). Circulation anomalies associated with TSPT+ over mid-high latitude North America and Western Atlantic represent a similar NAO-like meridional dipole mode, in accordance with that TSPT and NAO have a weak linear correlation of −0.23. Therefore, TSPT+ and NAO− generate a linear amplification effect over North America and Western Atlantic during NAO −⊕TSPT +, representing a stronger NAO-like circulation than that during NAO−\TSPT + (Fig. 5d). However, circulation responses to TSPT+ and NAO− exhibit distinct characteristics over the eastern North Atlantic and Europe as depicted in Fig. 5a and Fig. 5b. Thus, the significantly enhanced low pressure in the eastern North Atlantic and western Europe during NAO−⊕TSPT + (Fig. 5e) may associated with nonlinear interaction between NAO− and TSPT +. Furthermore, the contribution of nonlinear effect and linear superposition of NAO− and TSPT+ to the anomalously low over the studied area are comparable (Fig. 5f). This suggests that the relationship between NAO−, TSPT + and the NAE circulation involves complex dynamic processes. This synergistic effect on anomalously low over British Isles favors the nonlinear response of precipitation over southwestern Europe (Fig. 4e).

The circulation anomaly accompanies with zonal wind variation. Figure 6 shows the upper-level zonal wind anomaly and stationary Rossby wave activity flux in DJF which reflects the propagation of stationary Rossby waves and the direction of energy propagation[47]. It can be found that under isolated events, NAO− is associated with strengthening of the subtropical jet stream and wave activity in the NAE region (Fig. 6a), while TSPT+ is associated with those enhancements over Pacific and North America (Fig. 6b). Under the joint events, anomalous westerly jet stream and wave activity over the NAE region are significantly stronger than those during the isolated events. As shown in Fig. 6d, the linear superposition of NAO− and TSPT+ causes the subtropical westerly jet streams in the Pacific, North American and Atlantic regions to connect. Particularly, nonlinear effect of NAO− and TSPT+ on the westerly jet stream and wave activity over the NAE during NAO−⊕TSPT + contributes to a strengthened westerly anomaly and southeastward wave activities over East Atlantic and Western Europe (Fig. 6e). This synergistic effect is corresponded to that of circulation in Fig. 5. In addition, wave activities during the joint events propagate from southern

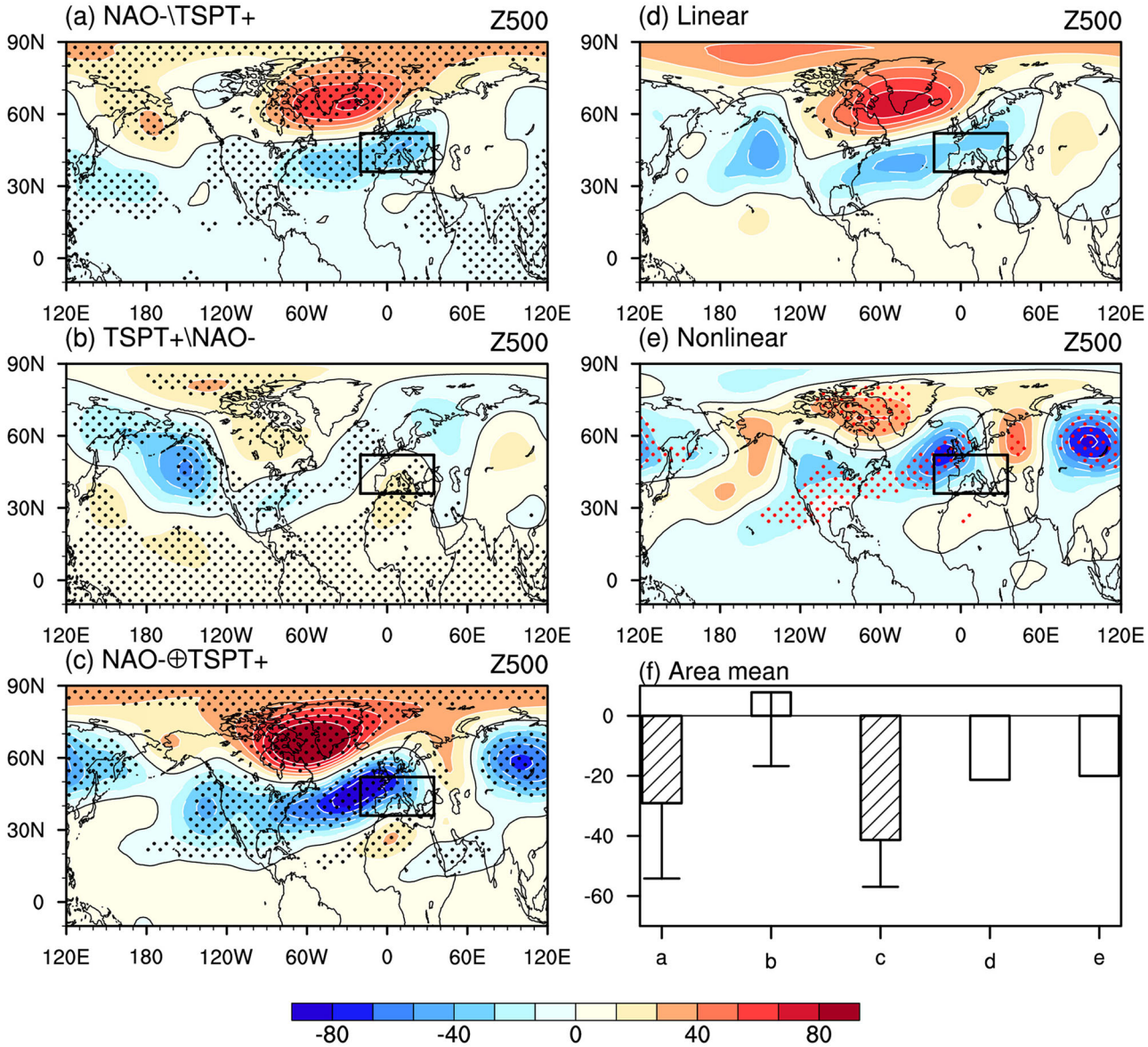

Fig. 5 | DJF geopotential height at 500 hPa. Composite mean anomalies of geopotential height (shading; gpm) at 500 hPa for **a** NAO−\TSPT+, **b** TSPT+\NAO−, **c** NAO−⊕TSPT+, **d** linear superposition of (**a**, **b**), **e** difference between (**c**, **d**). Bars in (**f**) indicate area mean values of the geopotential height anomalies in the black box in (**a**–**e**). Dotted areas in (**a**–**c**) are significant at or above the 90% confidence level. Red dotted areas in (**e**) indicate amplitude of geopotential height anomalies in (**c**) are significantly stronger than those in (**a**, **b**). Black slash bars in (**f**) indicate composites to climatology are significant at the 90% confidence level. The line variation over the bar in (**f**) indicates standard deviation.

Greenland southeastward to the subtropical Atlantic and Mediterranean region (Fig. 6c), corresponding to a stronger tripole circulation anomaly over the NAE region during NAO−⊕TSPT + (Fig. 6e). This enhancement of wave activity fluxes over the NAE region is mainly related to the complex nonlinear effect of NAO− and TSPT+ over the NAE region (Fig. 6e). Specifically, the nonlinear effect goes beyond linear superposition effect over the studied area (Fig. 6f), suggesting the nonlinear interaction of NAO− and TSPT+ in this region is non-negligible.

To further investigate the synergistic effect of NAO− and TSPT+ on the wave energy propagation, and to explore how TSPT+ influences the NAE region, Rossby wave ray tracing method is employed. This allows for the detection of the trajectories and pathways along which Rossby wave energy is excited by NAO− and TSPT + . Considering the persistence of autumn TSPT+ into winter, we will further analyze the wave ray initiated by DJF TSPT+ and NAO−. Figure 7 shows the DJF stationary Rossby wave ray trajectories initiated from wave sources in South Greenland and TSPT region. As displayed in Fig. 7, Rossby wave ray initiated from South Greenland propagates southeastward to South Europe and the Mediterranean region, which is similar with that of wave activity flux. Wave rays initiated from TSPT+ region especially from tropical and subtropical South Pacific can propagate across the tropical regions and then propagate towards the NAE region, suggesting that DJF TSPT+ can influence the North America and NAE circulation through atmospheric teleconnection. In particular, during TSPT + \NAO−, there are only a few wave rays associated with DJF TSPT+ that propagates to the NAE region. However, a significant increase of wave rays reaching the NAE region is observed during TSPT + ⊕NAO− (Fig. 7c). This might be related to that stronger westerly wind over subtropical Pacific, North America and NAE region during TSPT + ⊕NAO− is conducive to the wave energy propagating from Pacific downward to the NAE region. In addition, DJF SSTA over tropical Pacific during TSPT + ⊕NAO− is not significantly weaker than that during TSPT +

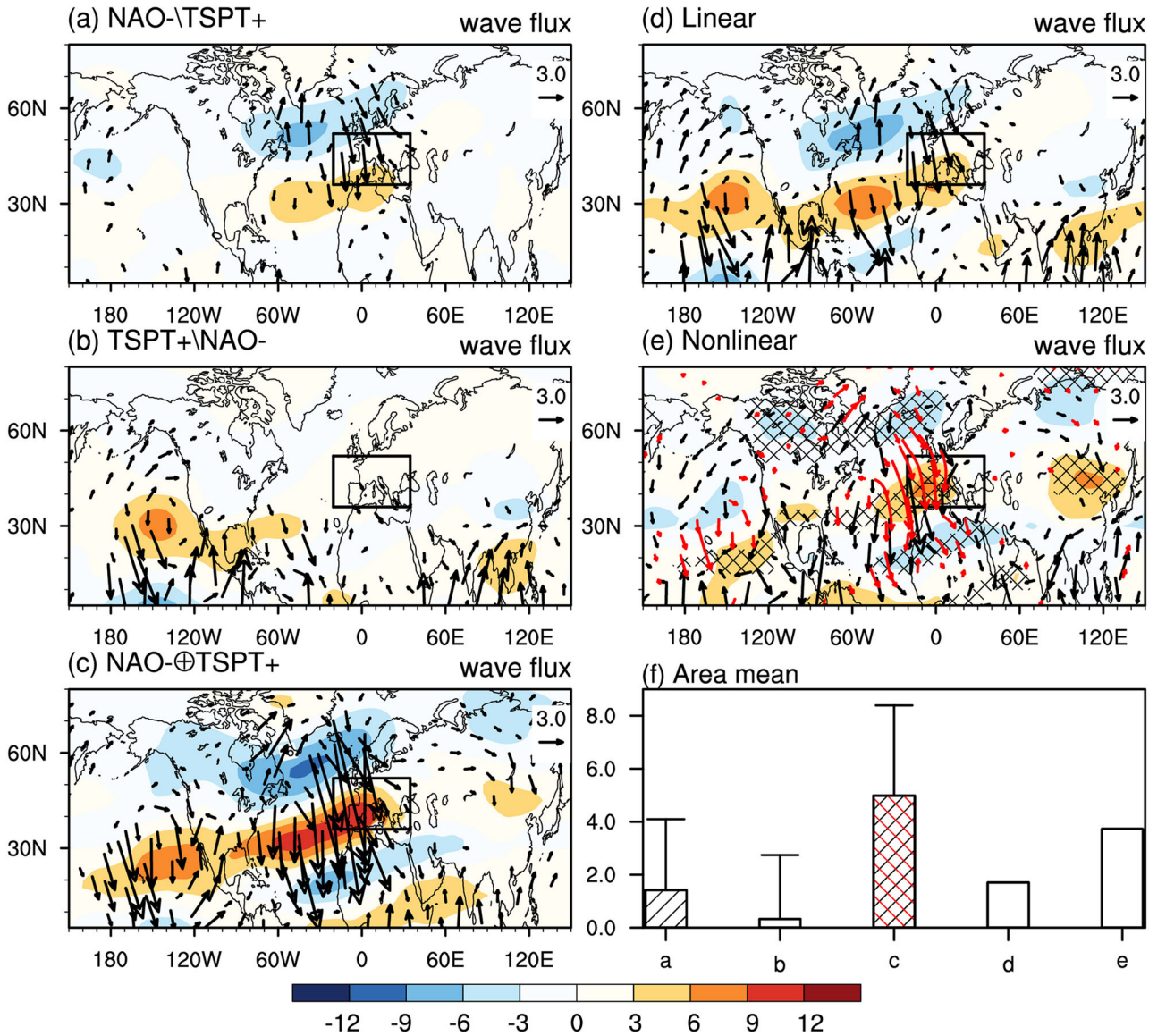

Fig. 6 | DJF wave activity flux and zonal wind at 200 hPa. Composite anomalies of DJF wave activity flux (arrows; $m^2 s^{-2}$) and zonal wind anomalies (contours; $m s^{-1}$) at 200 hPa for **a** NAO−\TSPT+, **b** TSPT+\NAO−, **c** NAO−⊕TSPT+, **d** linear superposition of (**a**, **b**), **e** difference between (**c**, **d**). Bars in (**f**) indicate area mean values of the wave activity fluxes in the black box in (**a**–**e**). Vectors < 0.5 $m^2 s^{-2}$ are omitted. Red arrows in (**e**) indicate values in (**c**) are significantly greater than those in (**a**, **b**). Crossed areas in (**e**) indicate zonal wind at 200 hPa in (**c**) are significantly stronger than those in (**a**) and (**b**). Black slash bars in (**f**) indicate composites to climatology are significant at the 90% confidence level, and red slash bar in (**f**) indicates composite in (**c**) is significantly stronger than that in (**a**). The line variation over the bar in (**f**) indicates standard deviation.

\NAO−, implying that the increase of DJF wave rays associated with TSPT+ during TSPT + ⊕NAO− is not induced by the intensity of ENSO. In general, DJF TSPT+ without NAO− has limited impact on the NAE region through Rossby wave energy propagation, but it has a clear and evident influence on the NAE region with NAO−. This suggests the existence of a nonlinear interaction between DJF TSPT+ and NAO− with regards to Rossby wave energy over the NAE region. This explains the result of circulation anomalies in Fig. 5c.

To further validate the nonlinear contributions of NAO− and TSPT+ on circulation over South Europe, we conducted a 50-year run of sensitivity experiment on the boreal autumn and winter SSTA in the equatorial and South Pacific (70°S-10°N, 160°E-270°E) during the TSPT+ as forcing (EXP1), and another 50-year run experiment of climatology state of SST as a control run and isolated events of NAO− (EXP0); the last 45 years run of EXP0 and EXP1 are used in this study. The isolated events of NAO− in the model is obtained from EXP0 when the normalized NAO index is smaller than −0.7, and events of TSPT + \NAO− and NAO−⊕TSPT + in the model is calculated from EXP1 when the normalized NAO index is greater and smaller than 0.7, respectively. By comparing the simulation results of the joint events and isolated events, we can assess the extent to which NAO− and TSPT + contribute nonlinearly to the circulation changes over East Atlantic and South Europe. It can be found that NAO− can be simulated in the atmospheric internal dynamic process (Fig. 8a). A tripole pattern (pos-neg-pos) of pressure anomaly over tropical and South Pacific is simulated under the forcing of TSPT+ (Fig. 8b, c). Under TSPT + \NAO−, abnormally weak and non-significant low appears in South Europe and the Mediterranean region (Fig. 8b), which is consistent with observation that TSPT + \NAO− have a weak influence on South Europe. In comparation, the simulation of TSPT+ forcing with NAO− sees a notably stronger NAO− like circulation (Fig. 8c), although circulation pattern does exhibit some deviation from the observed

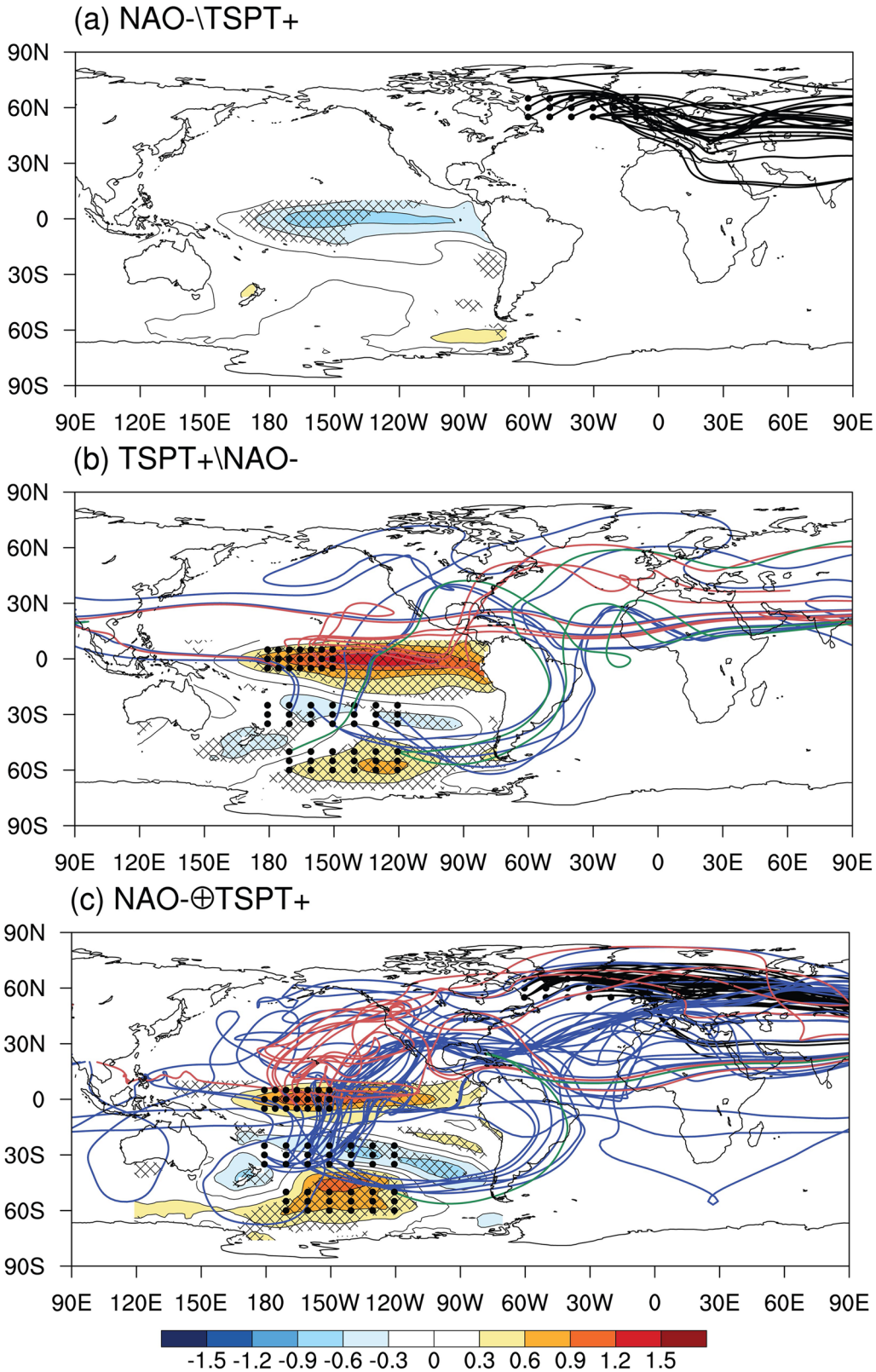

Fig. 7 | DJF stationary Rossby wave ray trajectories. DJF stationary Rossby wave ray trajectories and the evolution of total wavenumber initiated with zonal wavenumber 3–5 (green curves) at 200 hPa for sources corresponding to NAO− (black dots in North Atlantic) and DJF TSPT + (black dots in tropical and southern Pacific), respectively. **a** NAO−\TSPT+, **b** TSPT+\NAO−, **c** NAO−⊕TSPT+.

patterns (Fig. 5c). In terms of impact on anomalous low over South Europe, the linear superposition effect of NAO− and TSPT+ is found to be stronger (Fig. 8d, e, f). However, it is important to note that the simulation captures the nonlinear effect of NAO− and TSPT + , resulting in an anomalous low over southern Europe (Fig. 8e). The results of simulation confirm that boreal autumn and winter TSPT+ and winter NAO− have a significant synergistic effect on the circulation over the NAE region.

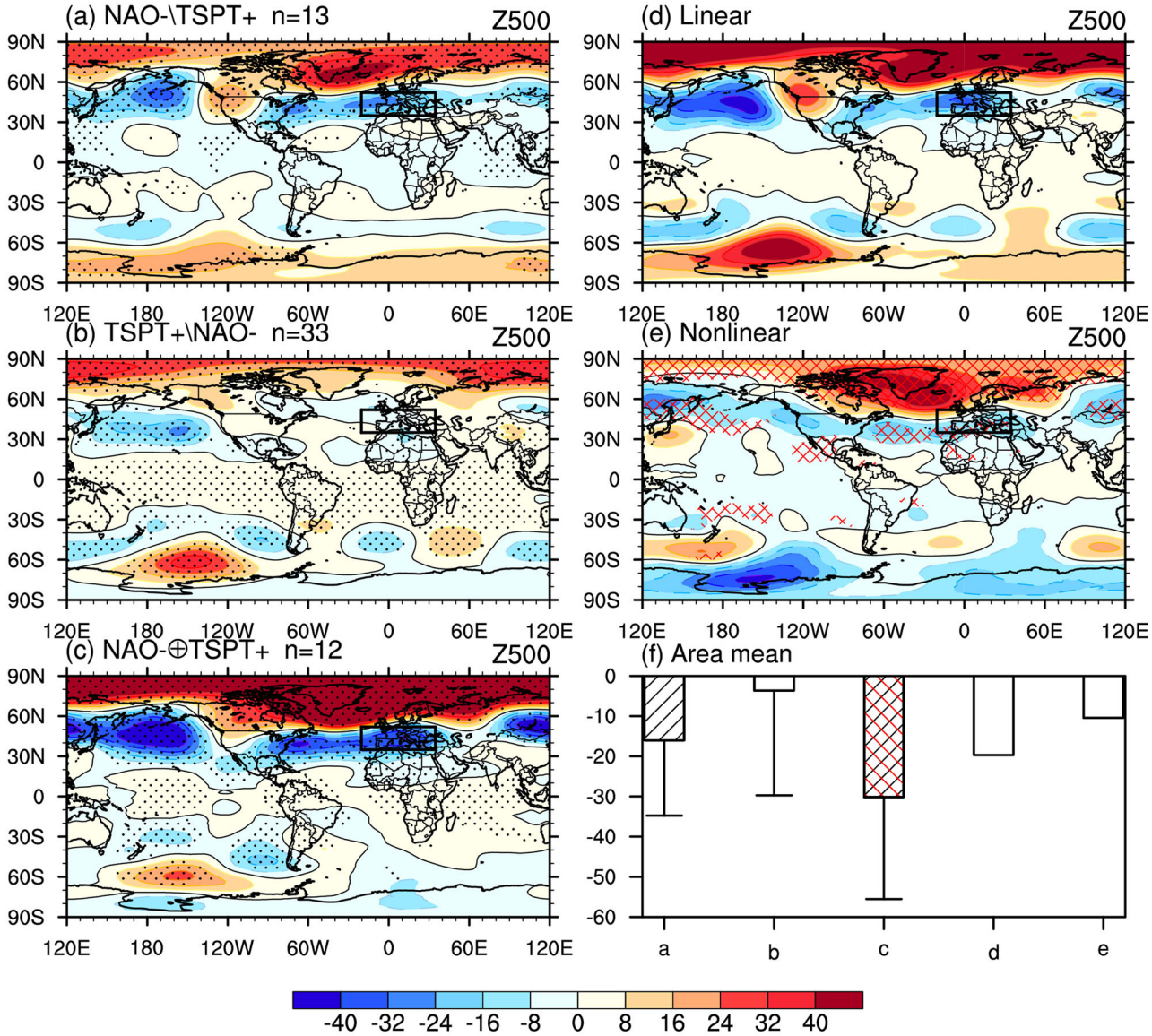

Fig. 8 | DJF geopotential height at 500 hPa from CAM5 simulation. Composite anomalies of DJF geopotential height (shading; gpm) at 500 hPa from EXP0 (**a**) and EXP1 (**b**–**c**) for **a** NAO−\TSPT+, **b** TSPT+\NAO−, **c** NAO−⊕TSPT+, **d** linear superposition of (**a**, **b**), **e** difference between (**c**, **d**). Bars in (**f**) indicate area mean values of the geopotential height anomalies in the black box in (**a**–**e**). Black dotted areas in (**a**–**c**) indicate composites to EXP0 are significant at the 90% confidence level. "*n*" in (**a**–**c**) indicates the number of composite events. Red crossed areas in (**e**) indicate composites in (**c**) are significantly stronger than those in (**a**, **b**) at the 90% confidence level. Black slash bars in (**f**) indicate composites to climatology are significant at the 90% confidence level, and red slash bar in (**f**) indicates composite in (**c**) is significantly stronger than that in (**a**). The line variation over the bar in (**f**) indicates standard deviation.

Synergistic effect of NAO− and TSPT+ on SEWP formation

It crucial to investigate how these enhanced circulation patterns ultimately influence SEWP. Figure 9 shows composites of winter integrated water vapor transport (IVT). Westly anomaly from subtropical North Atlantic transport moisture to the Mediterranean and further cyclonically transports to southern Europe under NAO−\TSPT + (Fig. 9a). During TSPT + \ NAO−, influenced by the anomalous low in northern Europe and anomalous high over North Africa and the Mediterranean (Fig. 5b), water vapor transports southeastward from Atlantic to the British Isles and the Alps, resulting in an increase in precipitation in the British Isles and Germany (Fig. 3b). During the joint events, the mid latitude cyclonic circulation over the Atlantic to western Europe significantly enhanced compared to the isolated events (Fig. 5c), resulting in a significant IVT increase from the Atlantic to South Europe and the Mediterranean region (Fig. 9c). As a result, linear superposition impact of NAO− and TSPT+ on the IVT over South Europe is weak (Fig. 9d). However, the nonlinear effect of NAO− and TSPT + on the circulation over the NAE region can lead to a stronger cyclonic IVT from the East Atlantic (Fig. 9e), which in turn contributes to the nonlinear response to SEWP (Fig. 3e).

As transient eddies play an important role in NAO− associated moisture transport[42], we further evaluate the transient eddy at lower level where moisture is concentrated. Figure 10 shows the transient eddies ($\overline{v'^2}$) at 850hPa. A meridional pattern of anomalous $\overline{v'^2}$ over the NAE region is seen during NAO−⊕TSPT +, with a clear strong $\overline{v'^2}$ anomaly extending northeastward from Southeastern United States, North Atlantic to South Europe (Fig. 10c). Comparatively, $\overline{v'^2}$ anomalies associated with NAO−\TSPT + and TSPT + \NAO− over the NAE region are characterized by different patterns, and the intensifies over the studied region are not significant (Fig. 10a, b). Thus, it is mainly the nonlinear effect of NAO− and TSPT+ contributes to the amplification of $\overline{v'^2}$ during the NAO−⊕TSPT + (Fig. 10e, f). Moreover, NAO− and TSPT+ have a synergistic effect on the

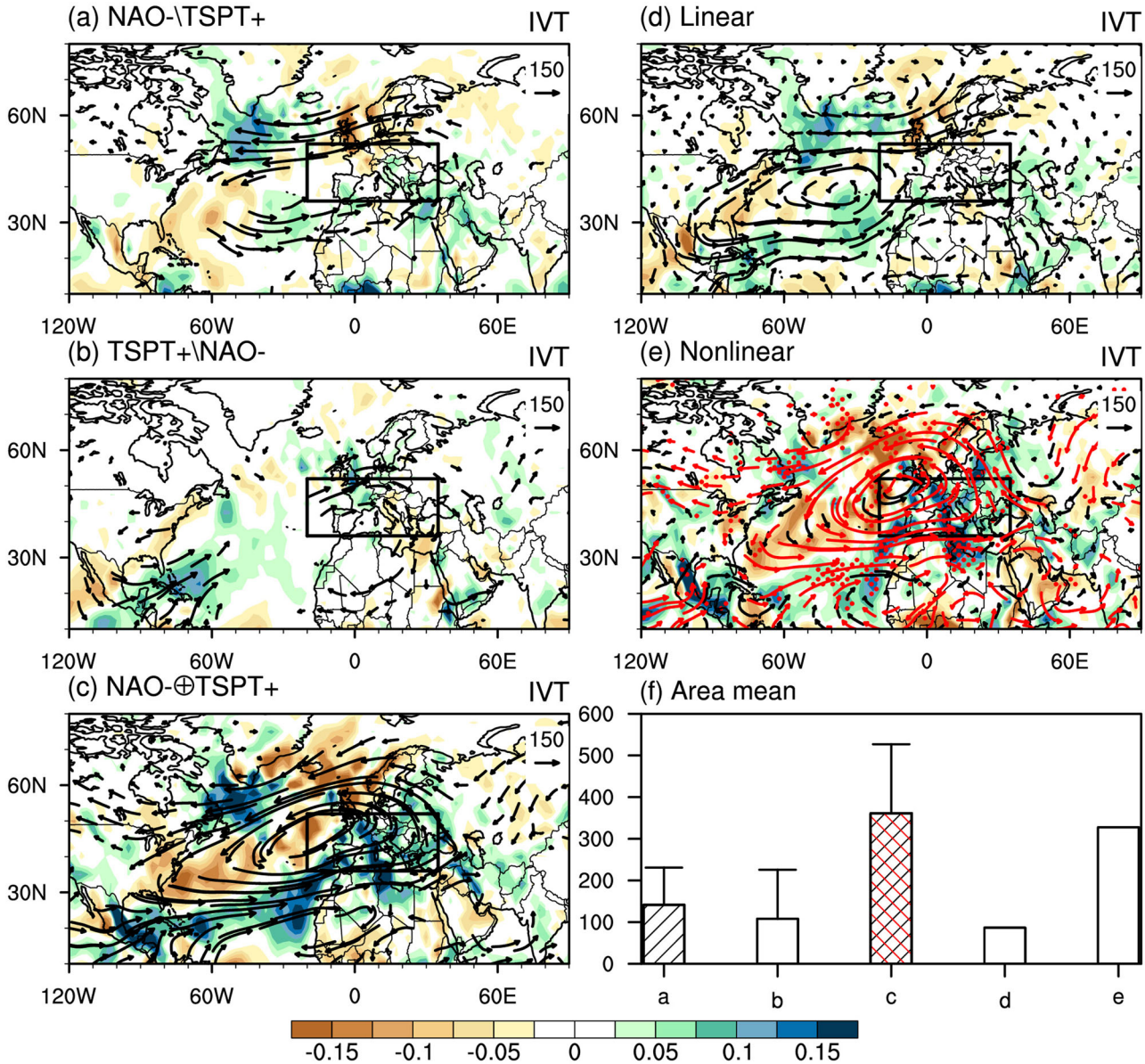

Fig. 9 | DJF integrated water vapor transport and divergence. Composites anomalies of DJF integrated water vapor transport (vectors; g kg^{-1} m s^{-1}) and divergence (*−1; shading; −10^{-6} g kg^{-1} s^{-1}) for **a** NAO−\TSPT+, **b** TSPT+\NAO−, **c** NAO−⊕TSPT+, **d** linear superposition of (**a**, **b**), **e** difference between (**c**, **d**). Bars in (**f**) indicate area mean values of integrated water vapor transport anomalies in the black box in (**a**–**e**). Shading areas are significant at the 90% confidence level, and red arrows and red dotted areas in (**e**) represent variables in (**c**) are significantly stronger than those in (**a**, **b**). Black slash bars in (**f**) indicate composites to climatology are significant at the 90% confidence level, and red slash bar in (**f**) indicates composite in (**c**) is significantly stronger than that in (**a**). The line variation over the bar in (**f**) indicates standard deviation.

upper tropospheric westerly jet in the subtropical Atlantic to southern Europe (Fig. 6c), which is conducive to storm activities[42].

Discussion

This paper reveals that a positive phase of meridional tripole mode (pos-neg-pos) of SSTA in tropical and southern Pacific in boreal autumn can persist into winter and has a synergistic effect on the SEWP increase with DJF NAO−. NAO− is associated with precipitation increase especially in the Mediterranean. In comparation, TSPT+ has a weaker relationship with SEWP than NAO−. TSPT + is associated with weak precipitation increase in British Isled, France and Germany, and anomalous weak dry conditions in the region south of 45°N. During the co-occurrence of TSPT+ and NAO −, the impact on SEWP is amplified, resulting in SEWP that are two times stronger than when they occur isolation. Furthermore, joint events of TSPT + with NAO− is indicative to SEWP occurrence than without NAO−, positive SEWP year account for 100% of joint events. Specifically, the enhancement of SEWP is attributed to the nonlinear interaction of NAO− and TSPT+ on SEWP rather than their superposition.

Large scale circulation analysis finds that during NAO−⊕TSPT +, northwest-southeast trend tripole like circulation anomaly in the NAE region is evidently strong. The strong circulation over the NAE region during NAO−⊕TSPT + is attributed to linear superposition responses of NAO− and TSPT+ which is similar with that of NAO−\TSPT +, and nonlinear effect exhibiting with an anomalous enhanced cyclonic circulation over East Atlantic and Britain Isles. The synergistic effect on the mean circulation over the NAE region accompanies with intensification of subtropical westerly jet from Atlantic to South Europe and intensified stationary waves propagating southeastward from Greenland to southern Europe and the Mediterranean. Dynamical mechanisms reveal that SON TSPT+ can persist into DJF, and DJF TSPT+ with NAO− excites obviously stronger

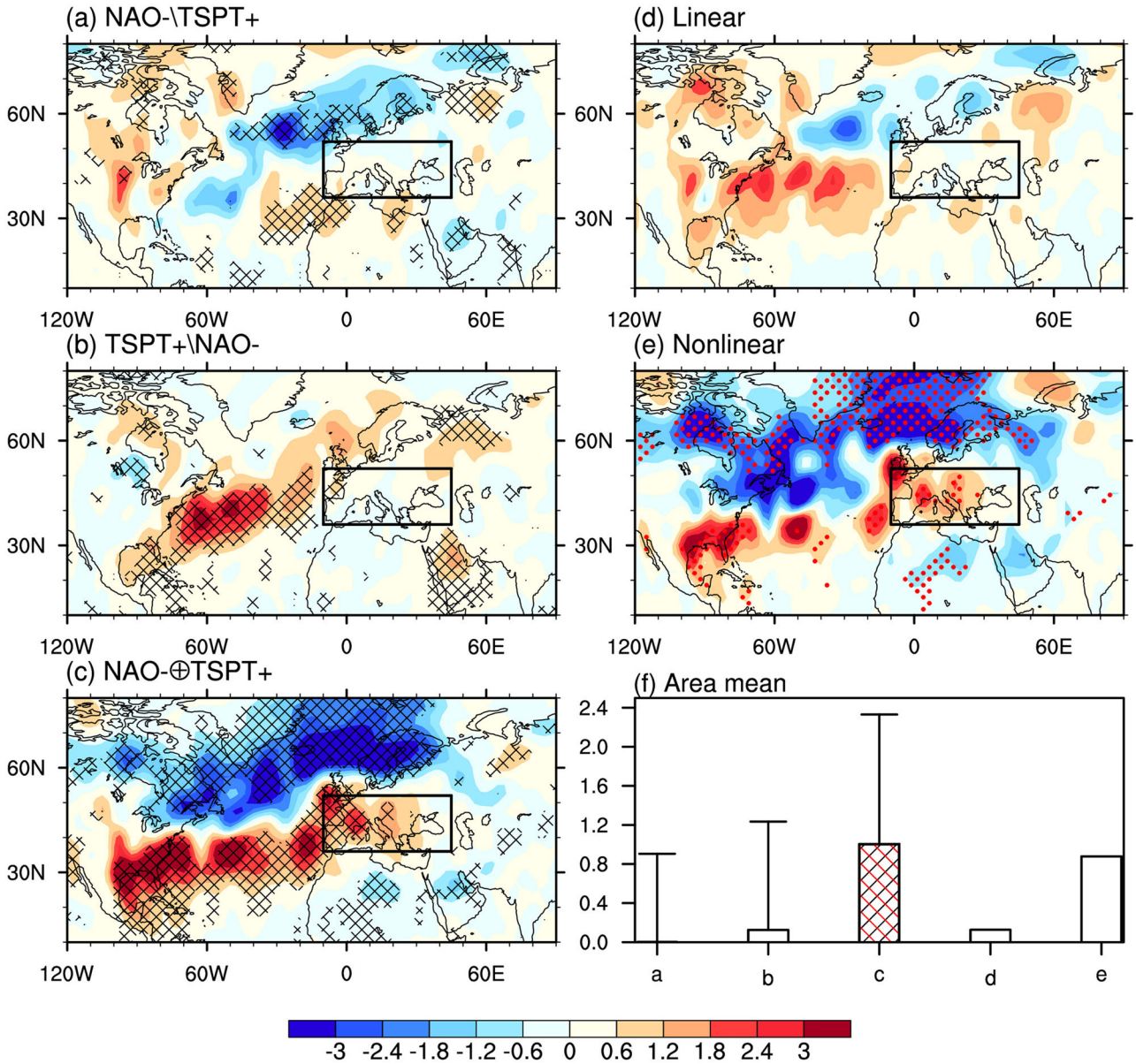

Fig. 10 | DJF $\overline{v'^2}$ at 850 hPa. Composites of DJF $\overline{v'^2}$ (m^{-2} s^{-2}) anomalies at 850 hPa for **a** NAO−\TSPT+, **b** TSPT+\NAO−, **c** NAO−⊕TSPT+, **d** linear superposition of (**a**, **b**), **e** difference between (**c**, **d**). Bars in (**f**) indicate area mean values in the black box in (**a**–**e**). Crossed areas in (**a**–**c**) are significant at or above the 90% confidence level. Red dotted areas in (**e**) indicate the amplitude of anomalies in (**c**) are significantly stronger than those in (**a**, **b**). Black slash bar in (**f**) indicates composites to climatology are significant at the 90% confidence level, and red slash bar in (**f**) indicates composite in (**c**) is significantly stronger than that in (**a**). The line variation over the bar in (**f**) indicates standard deviation.

Rossby wave energy propagating from South Pacific to the NAE region than that without NAO−. This suggests that TSPT+ can synergistically influence NAE region with NAO− through atmospheric teleconnection. Moreover, numerical simulation confirms that TSPT+ forcing with NAO− sees stronger NAO−like circulation anomaly, and the nonlinear effect on the abnormal low over midlatitude North Atlantic and southern Europe is stimulated. The synergistic effect of NAO− and TSPT+ on the mean circulation enhancing the water vapor transports and transient eddy over southern Europe, which favors the increase of SEWP.

The synergistic effect of NAO− and TSPT+ revealed in this study is valuable in terms of our understanding of SEWP variability. The synergistic effect in this study is detected by linear superposition and nonlinear effect. Numerical simulation results demonstrated that regardless of other external forcing, the autumn to winter forcing of TSPT+ with DJF NAO− can produce significantly amplified DJF circulation over East Atlantic and southern Europe. The potential for nonlinear interaction between TSPT+ and NAO− may be related to the complex internal atmospheric dynamics of wave–wave and/or wave–mean flow interaction. Despite the lack of clarity regarding the specific physical processes involved in the nonlinear interaction between NAO− and TSPT + , this study affirms the presence of the nonlinear interaction between NAO− and TSPT+ on the East Atlantic and Europe circulation, as well as SEWP. This finding also enhances our understanding of the complex relationships between multiple climate variables and the specified dynamical process, which provides potential implication for the study of nonlinear interaction in the observation.

As SSTA during TSPT+ is similar with El Niño (ENSO +), we further found 4 of the 20 years of strong positive TSPT events are non-ENSO events (Supplementary table 1), indicating that TSPT+ is not equivalent to

ENSO + . It is that ENSO+ plays an important role in the synergistically influence of TSPT+ and NAO− on southern Europe, while the role of SSTA over South Pacific on the synergistic effect is not to be ignored. The contribution of ENSO+ on the synergistic effect of TSPT+ and NAO− on SEWP can be examined in the future by comparing the numerical simulation of SST forcing imposed by ENSO+ and TSPT + , respectively.

Methods

Observational data

The gridded (mapped) observations in this study are focused on boreal winter monthly rainfall across Europe (see Fig. 1a) from December to February in the years from 1950 to 2018. The Global Precipitation Climatology Center monthly precipitation dataset (GPCC) with a 1° × 1° global grid was used. Atmospheric variables were obtained from the National Centers for Environmental Prediction–National Center for Atmospheric Research reanalysis dataset with a horizontal resolution of 2.5° × 2.5°. We also use the extended reconstructed sea surface temperature (ERRST v5) (SST)[48] from the National Climatic Data Center of the National Oceanic and Atmospheric Administration (NOAA). The NAO index is defined as the difference in normalized zonally averaged SLP over the North Atlantic region (80°W–30°E) between 35°N and 65°N[46].

Numerical simulation

To investigate the influences of the preceding boreal autumn and winter (September to February) SSTA, numerical simulations were performed with the Community Atmosphere Model Version 5 (CAM5). The "F_2000" component set is selected for CAM5, which uses a prescribed climatology for SST and sea ice and an active land model (CLM), coupled with CAM5. The simulations use a 1.9° (lat) ×2.5° (lon) horizontal grid resolution, with a 26 hybrid sigma pressure levels.

We design two CAM5 experiments using different lower boundary conditions: one control and one forcing simulations that are designed to investigate sensitivity to SSTA-forcing and synergistic effect of NAO and SSTA. In this paper, NAO is simulated by forcing of global climatology SST (EXP0), as multiple atmospheric circulation models driven by climatology sea surface temperature can simulate Arctic Oscillation have been confirmed[49–51], and interannual variability of the NAO can be explained in terms of climate "noise" and does not require forcing external to the atmosphere[1], despite forcing of Atlantic SST has an influence on the phase of NAO[43]. The method to calculate the NAO in the model is the same as those used for the observations[46]. The influence of preceding SSTA pattern is simulated by superimposing studied SSTA pattern (September to February) onto global climatology SST in the CAM5 (EXP1).

Definition of synergistic effect

The synergistic effects of forcing and physical processes used in this study is the same as previous studies[36–41]. Let A and B be the forcing events, in which $A \oplus B$ represents the co-occurrence events when both A and B occur, and $A \backslash B$ indicates the isolated events when A occurs without B. Similarly, $B \backslash A$ indicates the isolated events when B occurs without A. For a certain atmospheric response y (e.g., precipitation or other physical quantities), let y_1 denote its response during $A \backslash B$ event, y_2 denote its response during $B \backslash A$ event, and y_{12} denote its response during the events $A \oplus B$. If $|\overline{y_{12}}|$ is significantly greater than the maximum of $|\overline{y_1}|$ and $|\overline{y_2}|$, A and B have a synergistic effect on y; if $|\overline{y_{12}}|$ is less than the minimum of $|\overline{y_1}|$ and $|\overline{y_2}|$, A and B have an antagonistic effect on y[36]. When y_{12}, y_1 and y_2 are of the same sign, their synergistic effect from A and B is explicit synergism; otherwise, there might be an implicit synergistic effect[36]. The linear regression of B (A) on the monthly anomalies are removed before compositing $A \backslash B$ ($B \backslash A$), to better isolate the isolated influence of $A \backslash B$ ($B \backslash A$) Tang et al.[38]. We define the events being strong positive (negative) when the normalized index is above (below) 0.7 (− 0.7) considering both the significance and the number of positive (negative) events.

To further understand the synergistic effect of two forcing, the response of joint events can be expressed as follows:

$$y_{12} = y(A) + y(B) + y(A, B), \tag{1}$$

in which $y(A) + y(B)$ represents a linear superposition of responses of A\B and B\A events, indicating the linear superposition effect of A and B on y, the last term indicates the nonlinear effect of A and B on y.$y(A, B)$ is obtained by the difference between the joint event response (y_{12}) and the sum of responses of isolated events.

In this study, to measure the relationship between forcing and response anomalies to climatology for discontinuous events (isolated and joint events), local covariance is defined as follows:

$$Cov(x, y) = \sum_{i}^{n} (x_i - \bar{x})(y_i - \bar{y})/n, \tag{2}$$

in which $\bar{x} = \frac{\sum_j^N x_j}{N}, \bar{y} = \frac{\sum_j^N y_j}{N}$, n indicates length of discontinuous events, N represents length of total time series.

Significance test

The bootstrap methods are used to determine the statistical significance of the anomalies in a composite relative to climatology and the difference between two composites. The statistical significance of synergistic effect is determined by bootstrap methods[52,53]. We utilize bootstrap methods by resampling all of the joint events and isolated events in the record 1000 times and examine the 10th and 90th percentiles from the synthetic distribution[38].

Diagnosis on moisture transport

Intense moisture transport is essential to formation of extreme precipitation. Integrated horizontal water vapor transport (***IVT***) quantifies the horizontal atmospheric moisture transport in a Eulerian framework, and this vector is defined as[54]

$$\boldsymbol{IVT} = g^{-1} \int_{P_{bottom}}^{P_{top}} q\boldsymbol{v} dp, \tag{3}$$

where g is the gravitational acceleration, q is the specific humidity, $\boldsymbol{v}$ is the horizontal wind, and p is pressure.

To examine the dynamical underpinnings of moisture transport, we investigate the variability of v'^2 at 850hPa in the lower troposphere where moisture is concentrated, and the prime denotes 2.5–6-day bandpass-filtered eddies.

Wave activity flux, Rossby wave ray

The TN wave activity flux, which is applicable for stationary or migratory quasi-trophic eddies in a zonally varying basic flow, can infer where a packet is emitted and absorbed[47]. This wave activity flux is based on a quasi-geostrophic potential vorticity equation that is linearized about a steady non-uniform basic-state wind.

The far-field atmospheric response to large-scale forcing in the atmosphere is dominated by external Rossby waves[55,56]. Stationary Rossby wave ray tracing is used in this study to reflect the stationary planetary and Rossby wave energy propagation originating from local forcing[57]. Here, the stationary Rossby wave ray tracing was taken from Li et al. (2015) and Zhao et al.[58–60], which are derived from the barotropic nondivergent vorticity equation and the basic flow is both zonal and meridional non-uniform in both latitude and longitude.

Data availability

All observational and reanalysis data are publicly available. The Global Precipitation Climatology Center monthly precipitation dataset (GPCC) is available at https://www.psl.noaa.gov/data/gridded/data.gpcc.html. The National Centers for Environmental Prediction/National Center for Atmospheric Research (NCEP/

NCAR) global reanalysis version 1 dataset is available at https://psl.noaa.gov/data/reanalysis/reanalysis.shtml. The sea surface temperature (SST) data were from the extended reconstructed sea surface temperature (ERRST v5) (SST) from the National Climatic Data Center of the National Oceanic and Atmospheric Administration (https://www.psl.noaa.gov/data/gridded/data.noaa.ersst.v5.html). The NAO index is available at http://lijianping.cn/dct/page/65610. The Niño 3.4 index is available at https://psl.noaa.gov/gcos_wgsp/Timeseries/Nino34/.

Code availability

The codes used for all the analyses and visualization are available upon reasonable request to the corresponding author.

Received: 20 January 2024; Accepted: 15 March 2024;
Published online: 23 March 2024

References

1. Feldstein, S. The timescale, power spectra, and climate noise properties of teleconnection patterns. *J. Clim.* **13**, 4430–4440 (2000).
2. Woollings, T. J., Hoskins, B., Blackburn, M. & Berrisford, P. A new Rossby wave-breaking interpretation of the North Atlantic Oscillation. *J. Atmos. Sci.* **65**, 609–626 (2008).
3. Rogers, J. North Atlantic storm track variability and its association to the North Atlantic Oscillation and climate variability of northern Europe. *J. Clim.* **10**, 1635–1647 (1997).
4. Baldwin, M. & Dunkerton, T. Stratospheric harbingers of anomalous weather regimes. *Science* **294**, 581–584 (2001).
5. Robertson, A. W., Mechoso, C. R. & Kim, Y. J. The influence of Atlantic sea surface temperature anomalies on the North Atlantic Oscillation. *J. Clim.* **13**, 122–138 (2000).
6. Watanabe, M. & Kimoto, M. Tropical–extratropical connection in the Atlantic atmosphere–ocean variability. *Geophys. Res. Lett.* **26**, 2247–2250 (1999).
7. Okumura, Y., Xie, S. P., Numaguti, A. & Tanimoto, Y. Tropical Atlantic air– sea interaction and its influence on the NAO. *Geophys. Res. Lett.* **28**, 1507–1510 (2001).
8. Zhang, W. et al. Impact of ENSO longitudinal position on teleconnections to the NAO. *Clim. Dyn.* **52**, 257–274 (2019).
9. Zhang, W. & Jiang, F. Subseasonal variation in the winter ENSO-NAO relationship and the modulation of tropical North Atlantic SST variability. *Climate* **11**, 47 (2023).
10. Zorita, E., Kharin, V. & von Storch, H. The atmospheric circulation and sea surface temperature in the North Atlantic area in winter: Their interaction and relevance for Iberian precipitation. *J. Clim.* **5**, 1097–1108 (1992).
11. Marshall, J. et al. North Atlantic climate variability: Phenomena, impacts and mechanisms. *Int. J. Climatol.* **21**, 1863–1898 (2001).
12. Trigo, R. M., Osborn, T. J. & Corte-Real, J. M. The North Atlantic oscillation influence on Europe: Climate impacts and associated physical mechanisms. *Clim. Res.* **20**, 9–17 (2002).
13. Trigo, R. et al. Relations between variability in the Mediterranean region and mid-latitude variability. *Mediterr. Clim. Var.* **4**, 179–226 (2006).
14. Hurrell, J. W., Kushnir, Y., Ottersen, G. & Visbeck, M. An overview of the North Atlantic Oscillation. *Geophys. Monogr. Ser.* **134**, 1–35 (2003).
15. Wibig, J. Precipitation in Europe in relation to circulation patterns at the 500 hPa level. *Int. J. Climatol.* **19**, 253–269 (1999).
16. Queralt, S. et al. North Atlantic Oscillation influence and weather types associated with winter total and extreme precipitation events in Spain. *Atmos. Res.* **94**, 675–683 (2009).
17. Muñoz-Díaz, D. & Rodrigo, F. S. Seasonal rainfall variations in Spain (1912–2000) and their links to atmospheric circulation. *Atmos. Res.* **81**, 94–110 (2006).
18. Xoplaki, E. Climate variability over the Mediterranean, PhD thesis, University of Bern, Switzerland, http://sinus.unibe.ch/klimet/docs/phd_xopla-ki.pdf (2002).
19. Ding, S., Chen, W., Feng, J. & Grafa, H. F. Combined impacts of PDO and two types of La Niña on climate anomalies in Europe. *J. Clim.* **30**, 3253–3278 (2017).
20. Kalimeris, A., Ranieri, E., Founda, D. & Norrant, C. Variability modes of precipitation along a Central Mediterranean area and their relations with ENSO, NAO, and other climatic patterns. *Atmos. Res.* **198**, 56–80 (2017).
21. Hatzaki, M. & Wu, R. The south-eastern Europe winter precipitation variability in relation to the North Atlantic SST. *Atmos. Res.* **152**, 61–68 (2015).
22. Pozo-Vázquez, D., Gámiz-Fortis, S. R., Tovar-Pescador, J., Esteban-Parra, M. J. & Castro-Díez, Y. El Niño-Southern oscillation events and associated European winter precipitation anomalies. *Int. J. Climatol.* **25**, 17–31 (2005).
23. Shaman, J. & Tziperman, E. An atmospheric teleconnection linking ENSO and Southwestern European precipitation. *J. Clim.* **24**, 124–139 (2011).
24. Mezzina, B. et al. Tropospheric pathways of the late-winter ENSO teleconnection to Europe. *Clim. Dyn.* **60**, 3307–3317 (2022).
25. Zanchettin, D., Franks, S. W., Traverso, P. & Tomasino, M. On ENSO impacts on European wintertime rainfalls and their modulation by the NAO and the Pacific multi-decadal variability described through the PDO index. *Int. J. Climatol.* **28**, 995–1006 (2008).
26. Ropelewski, C. F. & Halpert, M. S. Global and regional scale precipitation patterns associated with the El Niño/Southern oscillation. *Mon. Wea. Rev.* **115**, 1606–1626 (1987).
27. Shaman, J. The seasonal effects of ENSO on European precipitation: Observational analysis. *J. Clim.* **27**, 6423–6438 (2014).
28. Tabari, H. & Willems, P. Lagged influence of Atlantic and Pacific climate patterns on European extreme precipitation. *Sci. Rep.* **8**, 5748 (2018).
29. Mezzina, B., García-Serrano, J., Bladé, I. & Kucharski, F. Dynamics of the ENSO teleconnection and NAO variability in the North Atlantic-European late winter. *J. Clim.* **33**, 907–923 (2020).
30. Mathieu, P.-P., Sutton, R. T., Dong, B. & Collins, M. Predictability of winter climate over the North Atlantic European Region during ENSO Events. *J. Clim.* **17**, 1953–1974 (2004).
31. Brönnimann, S. Impact of El Niño-Southern Oscillation on European Climate: ENSO Impact on Europe. *Rev. Geophys.* **45**, RG3003 (2007).
32. Molteni, F. & Brookshaw, A. Early- and late-winter ENSO teleconnections to the Euro-Atlantic region in state-of-the-art seasonal forecasting systems. *Clim. Dyn.* **61**, 2673–2692 (2023).
33. Benassi, M. et al. El Niño teleconnection to the Euro-Mediterranean late-winter: the role of extratropical Pacific modulation. *Clim. Dyn.* **58**, 2009–2029 (2022).
34. Liu, T., Li, J., Wang, Q. & Zhao, S. Influence of the autumn SST in the southern Pacific ocean on winter precipitation in the North American monsoon region. *Atmos. (Basel).* **11**, 1–14 (2020).
35. Ao, J. & Sun, J. The impact of boreal autumn SST anomalies over the South Pacific on boreal winter precipitation over East Asia. *Adv. Atmos. Sci.* **33**, 644–655 (2016).
36. Li, J. P., Zheng, F., Sun, C., Feng, J. & Wang, J. Pathways of Influence of the Northern Hemisphere Mid-high Latitudes on East Asian Climate: A Review. *Adv. Atmos. Sci.* **36**, 902–921 (2019).
37. An, X. D., Sheng, L. F. & Li, J. P. Synergistic effect of SST anomalies in the North Pacific and North Atlantic on summer surface air temperature over the Mongolian Plateau. *Clim. Dyn.* **56**, 1449–1465 (2021).
38. Tang, X. X., Li, J. P., Zhang, Y. Z., Li, Y. J. & Zhao, S. Synergistic Effect of El Nino and Negative phase of NAO on Winter Precipitation in the Southeastern United States. *J. Clim.* **36**, 1767–1791 (2023).

39. Sun, Y. & Li, J. Synergistic effect of El Niño and the North Pacific Oscillation on wintertime precipitation over Southeastern China and the East China Sea Kuroshio area. *Clim. Dyn.* **58**, 1635–1649 (2022).
40. Wang, H. et al. The synergistic effect of the preceding winter Northern Hemisphere annular mode and spring tropical North Atlantic SST on spring extreme cold events in the mid-high latitudes of East Asia. *Clim. Dyn.* **59**, 3175–3191 (2022).
41. Wang, H., Li, J., Zheng, F. & Li, F. The synergistic effect of the summer NAO and northwest pacific SST on extreme heat events in the central–eastern China. *Clim. Dyn.* **61**, 4283–4300 (2023).
42. Seager, R. et al. Mechanisms of winter precipitation variability in the european-mediterranean region associated with the North Atlantic Oscillation. *J. Clim.* **33**, 7179–7196 (2020).
43. Rodwell, M. J., Rowell, D. P. & Folland, C. K. Oceanic forcing of the wintertime North Atlantic Oscillation and European climate. *Nature* **398**, 320–323 (1999).
44. Hurrell, J. W. Decadal trends in the North Atlantic Oscillation regional temperatures and precipitation. *Science* **269**, 676–679 (1995).
45. Hurrell, J. W., Kushnir, Y., Ottersen, G. & Visbeck, M. An over- view of the North Atlantic Oscillation. The North Atlantic Oscillation: Climatic Significance and Environmental Impact. (eds. Hurrell, J. W., Kushnir, Y., Ottersen, G. & Visbeck, M.) **134**, 1–35 (2003).
46. Li, J. P. & Wang, J. X. L. A new North Atlantic Oscillation index and its variability. *Adv. Atmos. Sci.* **20**, 661–676 (2003).
47. Takaya, K. & Nakamura, H. A formulation of a phase- independent wave-activity flux for stationary and migratory quasigeostrophic eddies on a zonally varying basic flow. *J. Atmos. Sci.* **58**, 608–627 (2001).
48. Huang, B. et al. Extended Reconstructed Sea Surface Temperatures Version 5 (ERSSTv5): Upgrades, Validations, and Intercomparisons. *J. Clim.* **30**, 8179–8205 (2017).
49. Limpasuvan, V. & Hartmann, D. L. Eddies and the annular modes of climate variability. *Geophys. Res. Lett.* **26**, 3133–3136 (1999).
50. Limpasuvan, V. & Hartmann, D. L. Wave-maintained annular modes of climate variability. *J. Clim.* **13**, 4414–4429 (2000).
51. Yamazaki, K. & Shinya, Y. Analysis of the Arctic Oscillation simulated by AGCM. *J. Meteor. Soc. Jpn.* **77**, 1287–1298 (1999).
52. Deser, C., Simpson, I. R., McKinnon, K. A. & Phillips, A. S. The Northern Hemisphere extratropical atmospheric circulation response to ENSO: How well do we know it and how do we evaluate models accordingly? *J. Clim.* **30**, 5059–5082 (2017).
53. Deser, C., Simpson, I. R., Phillips, A. S. & McKinnon, K. A. How well do we know ENSO's climate impacts over North America, and how do we evaluate models accordingly? *J. Clim.* **31**, 4991–5014 (2018).
54. Newell, R., Newell, N., Zhu, Y. & Scott, C. Tropospheric rivers? A pilot study. *Geophys. Res. Lett.* **19**, 2401–2404 (1992).
55. Hoskins, B. J. & Karoly, D. J. The steady linear response of a spherical atmosphere to thermal and orographic forcing. *J. Atmos. Sci.* **38**, 1179–1196 (1981).
56. Wallace, J. M. & Gutzler, D. S. Teleconnections in the geopotential height field during the Northern Hemisphere winter. *Mon. Wea. Rev.* **109**, 784–812 (1981).
57. Hoskins, B. J. & Ambrizzi, T. Rossby wave propagation on a realis- tic longitudinally varying flow. *J. Atmos. Sci.* **50**, 1661–1671 (1993).
58. Li, Y., Li, J., Jin, F. F. & Zhao, S. Interhemispheric propagation of stationary rossby waves in a horizontally nonuniform background flow. *J. Atmos. Sci.* **72**, 3233–3256 (2015).
59. Zhao, S., Li, J. & Li, Y. Dynamics of an interhemispheric teleconnection across the critical latitude through a southerly duct during boreal winter. *J. Clim.* **28**, 7437–7456 (2015).
60. Zhao, S., Li, J., Li, Y., Jin, F. F. & Zheng, J. Interhemispheric influence of Indo-Pacific convection oscillation on Southern Hemisphere rainfall through southward propagation of Rossby waves. *Clim. Dyn.* **52**, 3203–3221 (2019).

Acknowledgements

We thank all the data providers. This work is supported by the National Natural Science Foundation of China (NSFC) Project (42288101 and 42130607), Laoshan Laboratory (No.LSKJ202202600), and Shandong Natural Science Foundation Project (ZR2019ZD12), Fundamental Research Funds for the Central Universities (201962009). We are thankful to Center for High Performance Computing and System Simulation, Pilot National Laboratory for Marine Science and Technology (Qingdao) for providing computing resource. The funder played no role in study design, data collection, analysis and interpretation of data, or the writing of this manuscript.

Author contributions

All authors contributed to the design of this work. X.T. analyzed and interpreted the data, and drafted this work. J.L. revised critically for important intellectual content. All authors agree on the completed version.

Competing interests

The authors declare no competing interests.

Additional information

Supplementary information The online version contains supplementary material available at https://doi.org/10.1038/s41612-024-00628-y.

Correspondence and requests for materials should be addressed to Jianping Li.